11-14-2017

A Comprehensive Patient-Derived Xenograft Collection Representing the Heterogeneity of Melanoma.

Clemens Krepler
Wistar Institute

Katrin Sproesser
Wistar Institute

Patricia Brafford
Wistar Institute

Marilda Beqiri
Wistar Institute

Bradley Garman
University of Pennsylvania

Authors

Clemens Krepler, Katrin Sproesser, Patricia Brafford, Marilda Beqiri, Bradley Garman, Min Xiao, Batool Shannan, Andrea Watters, Michela Perego, Gao Zhang, Adina Vultur, Xiangfan Yin, Qin Liu, Ioannis N Anastopoulos, Bradley Wubbenhorst, Melissa A. Wilson, Wei Xu, Giorgos Karakousis, Michael Feldman, Xiaowei Xu, Ravi Amaravadi, Tara C. Gangadhar, David E. Elder, Lauren E. Haydu, Jennifer A. Wargo, Michael A. Davies, Yiling Lu, Gordon B. Mills, Dennie T. Frederick, Michal Barzily-Rokni, Keith T. Flaherty, Dave S. Hoon, Michael Guarino, Joseph J. Bennett, Randall W. Ryan, Nicholas J. Petrelli, Carol L. Shields, Mizue Terai, Takami Sato, Andrew E. Aplin, Alexander Roesch, David Darr, Steve Angus, Rakesh Kumar, Ensar Halilovic, Giordano Caponigro, Sebastien Jeay, Jens Wuerthner, Annette Walter, Matthias Ocker, Matthew B. Boxer, Lynn Schuchter, Katherine L Nathanson, and Meenhard Herlyn

Cell Reports

Resource

A Comprehensive Patient-Derived Xenograft Collection Representing the Heterogeneity of Melanoma

Graphical Abstract

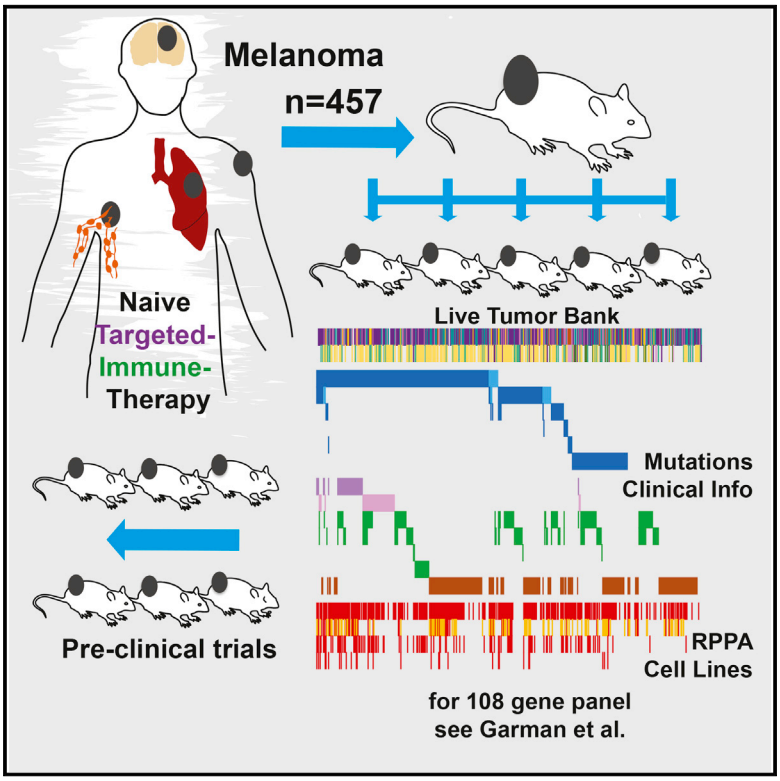

Authors

Clemens Krepler, Katrin Sproesser, Patricia Brafford, ..., Lynn Schuchter, Katherine L. Nathanson, Meenhard Herlyn

Correspondence

herlynm@wistar.org

In Brief

Krepler et al. have established a collection of melanoma patient-derived xenografts (PDX). Melanoma is a very heterogeneous cancer, and this large collection includes even rare subtypes and genetic aberrations in sufficient numbers. Multiple PDX from therapy-resistant patients are characterized and tested in pre-clinical trials for second line therapies.

Highlights

- Established directly from patients; largest collection to date
- Multiple PDX established from immune and targeted therapy-resistant patients
- Multiple PDX from brain metastasis samples
- Multiple PDX from rare subgroups and rare genetic aberrations

Krepler et al., 2017, Cell Reports *21*, 1953–1967
November 14, 2017
https://doi.org/10.1016/j.celrep.2017.10.021

CellPress

Cell Reports
Resource

OPEN ACCESS
CellPress

A Comprehensive Patient-Derived Xenograft Collection Representing the Heterogeneity of Melanoma

Clemens Krepler,[1] Katrin Sproesser,[1] Patricia Brafford,[1] Marilda Beqiri,[1] Bradley Garman,[2] Min Xiao,[1] Batool Shannan,[1] Andrea Watters,[1] Michela Perego,[1] Gao Zhang,[1] Adina Vultur,[1] Xiangfan Yin,[1] Qin Liu,[1] Ioannis N. Anastopoulos,[2] Bradley Wubbenhorst,[2] Melissa A. Wilson,[2] Wei Xu,[3] Giorgos Karakousis,[3] Michael Feldman,[3] Xiaowei Xu,[3] Ravi Amaravadi,[3] Tara C. Gangadhar,[3] David E. Elder,[3] Lauren E. Haydu,[4] Jennifer A. Wargo,[4] Michael A. Davies,[4] Yiling Lu,[4] Gordon B. Mills,[4] Dennie T. Frederick,[5] Michal Barzily-Rokni,[5] Keith T. Flaherty,[5] Dave S. Hoon,[6] Michael Guarino,[7] Joseph J. Bennett,[7] Randall W. Ryan,[7] Nicholas J. Petrelli,[7] Carol L. Shields,[8] Mizue Terai,[9] Takami Sato,[9] Andrew E. Aplin,[9] Alexander Roesch,[10,11] David Darr,[12] Steve Angus,[12] Rakesh Kumar,[13] Ensar Halilovic,[14] Giordano Caponigro,[14] Sebastien Jeay,[14] Jens Wuerthner,[14] Annette Walter,[15] Matthias Ocker,[15] Matthew B. Boxer,[16] Lynn Schuchter,[3] Katherine L. Nathanson,[2] and Meenhard Herlyn[1,17,*]

[1]Molecular and Cellular Oncogenesis Program, Wistar Institute, Philadelphia, PA 19104, USA
[2]Department of Medicine, Division of Translational Medicine and Human Genetics, Perelman School of Medicine, University of Pennsylvania, Philadelphia, PA 19104, USA
[3]Abramson Cancer Center, Perelman School of Medicine, University of Pennsylvania, Philadelphia, PA 19104, USA
[4]MD Anderson Cancer Center, University of Texas, Houston, TX 77030, USA
[5]Massachusetts General Hospital Cancer Center, Boston, MA 02114, USA
[6]Translational Molecular Medicine, John Wayne Cancer Institute, Santa Monica, CA 90404, USA
[7]Helen F. Graham Cancer Center at Christiana Care, Newark, DE 19713, USA
[8]Ocular Oncology Service, Wills Eye Hospital, Philadelphia, PA 19107, USA
[9]Sidney Kimmel Cancer Center, Thomas Jefferson University, Philadelphia, PA 19107
[10]Department of Dermatology, University Duisburg-Essen, University Hospital Essen, 45147 Essen, Germany
[11]German Consortium of Translational Cancer Research, Heidelberg, Germany
[12]Lineberger Cancer Center, University of North Carolina Chapel Hill, NC 27514, USA
[13]Glaxosmithkline, Collegeville, PA 19426, USA
[14]Novartis Institutes for Biomedical Research, Cambridge, MA 02139, USA
[15]Bayer Pharma AG, Berlin 13353, Germany
[16]National Center for Advancing Translational Sciences, NIH, Rockville, MD 20850, USA
[17]Lead Contact
*Correspondence: herlynm@wistar.org
https://doi.org/10.1016/j.celrep.2017.10.021

SUMMARY

Therapy of advanced melanoma is changing dramatically. Following mutational and biological subclassification of this heterogeneous cancer, several targeted and immune therapies were approved and increased survival significantly. To facilitate further advancements through pre-clinical *in vivo* modeling, we have established 459 patient-derived xenografts (PDX) and live tissue samples from 384 patients representing the full spectrum of clinical, therapeutic, mutational, and biological heterogeneity of melanoma. PDX have been characterized using targeted sequencing and protein arrays and are clinically annotated. This exhaustive live tissue resource includes PDX from 57 samples resistant to targeted therapy, 61 samples from responders and non-responders to immune checkpoint blockade, and 31 samples from brain metastasis. Uveal, mucosal, and acral subtypes are represented as well. We show examples of pre-clinical trials that highlight how the PDX collection can be used to develop and optimize precision therapies, biomarkers of response, and the targeting of rare genetic subgroups.

INTRODUCTION

Therapeutic options for advanced melanoma have improved from limited to approved kinase inhibitor and immune checkpoint therapy. 5-year survival rates have nearly doubled (Menzies et al., 2015; Schadendorf et al., 2015). Precision medicine and immune oncology are major areas of translational melanoma research. The complex melanoma landscape needs improved models reflecting all mutational and clinical subtypes. The UV carcinogenic etiology of melanoma makes it one of the most highly mutated cancers (Alexandrov et al., 2013). This high mutational burden may be the reason for the success of immune checkpoint blockade (Callahan et al., 2016), but makes developing rational "precision" therapies challenging (Krepler et al., 2016).

The Melanoma Cancer Genome Atlas (TCGA) includes comprehensive molecular characterization of 333 non-acral cutaneous melanomas and is an important resource. It confirmed

the main mutational subgroups of BRAF, NRAS, NF1, and triple wild-type (WT) and highlighted the distinct heterogeneity and high mutational burden of melanoma (Cancer Genome Atlas, 2015). Subtypes not included in the TCGA but published elsewhere are uveal (Van Raamsdonk et al., 2010), acral cutaneous (Furney et al., 2014), and mucosal melanoma (Sheng et al., 2016).

Patient-derived xenografts (PDX) as xenotransplantation of human tumors into athymic nude mice were first described by Rygaard and Povlsen (1969). PDX are directly established from patient tumors in immunodeficient mice and thus provide a source of tumor tissue closely resembling the clinical lesion (Hidalgo et al., 2014). Melanoma is uniquely suited to this approach as even single cells are tumorigenic *in vivo* (Quintana et al., 2008). Melanoma PDX were shown to accurately model the clinical disease and response to targeted therapy (Einarsdottir et al., 2014). We have shown recently that PDX derived from BRAF-inhibitor-relapsed patients and expanded on chronic therapy could be used to identify effective second-line combination therapies based on genomic and proteomic profiling (Krepler et al., 2016). Whereas these studies demonstrate the feasibility of the PDX approach, the melanoma TCGA and other studies (Arafeh et al., 2015; Cancer Genome Atlas, 2015; Krauthammer et al., 2015) highlight the pronounced heterogeneity of this cancer type. Both concepts are combined here in an unparalleled collection of 459 mutationally and clinically diverse melanoma PDX and live frozen tissues, providing an exhaustive and testable resource for the melanoma research field. This resource is highly clinically annotated and includes rare body sites and subtypes such as brain metastasis, uveal, mucosal, and acral melanoma, as well as pre- and post-therapy samples from targeted inhibitor- and checkpoint-blockade-treated patients.

RESULTS

Establishment of Melanoma PDX

We have collected 694 melanoma samples for PDX generation from eight institutions (Figure 1A). Fresh tumor samples were either directly implantated within 24 hr subcutaneously (s.c.) in NOD/SCID/IL-2Rγnull (NSG) mice or banked as cryopreserved live tissue (Figure 1A). Keeping primary tissue in a live tumor bank was a cost-effective alternative to fresh implantation but depended on adequate amounts of tissue. Both approaches successfully established PDX, and detailed methods are included in the Experimental Procedures and in a standard operating procedures (SOP) handbook (Data S1).

Of the samples collected, 319 were established as PDX and 140 were banked as live primary tissue (Figure 1B), totaling 459 models from 384 different patients. Failure to establish a PDX was due to sample contamination, unexpected death of a primary recipient animal, receipt of non-viable samples, or non-melanoma samples (Figure 1B). Thus, although the overall success rate for establishing melanoma PDX was 62%, the take rate corrected for these factors was 83% (Figure 1C). This excluded primary uveal samples whose take rate was 11%.

Time to Tumor Growth and Tumor Growth Rate

Tumor samples were obtained from fine-needle aspirates (FNA), core biopsies, or surgical excisions. We found no significant difference in latency (time from implantation to palpable tumor) and tumor growth rates (time to maximal tumor size) (Figures 1D and 1E).

Very Small Cell Numbers Are Needed to Establish a Melanoma PDX

Tissues from three patients were enzymatically digested, and hematopoietic cells, red blood cells, and endothelial cells were removed. We observed consistent tumor engraftment in mice at 1,000, 100, 10, and 1 cell(s)/ mouse (Figure 1F). The latency period was extended by up to 4 months indicating that a follow-up of 6 months is optimal to achieve maximum engraftment. Further, tumorigenicity did not significantly change when sorting the cells for the cancer stem cell marker CD271 (Boiko et al., 2010) (Figure 1G).

Patient Demographics Reflect the Clinical Spectrum of the Disease

Patient ages ranged from 20 to 89 years, with a peak between 60 and 69 years (Figure 2A). Male patients were predominant, likely representing our sampling bias for advanced disease (Geller et al., 2002) (Figure 2B). More than 80% of patients had stage IV disease. The largest proportion of samples (68%) was metastases from patients with non-acral cutaneous primaries (Figure 2C), but we also included 59 unknown primary, 17 mucosal, 15 acral cutaneous, and 10 uveal melanomas. Approximately 44% were s.c. (Figure 2D) and 26% lymph node metastasis samples, since these are often excised for diagnostic or therapeutic reasons. Remarkably, 23% were distant organ metastates, including brain. Primary melanomas represented 5%, although these were thick primaries and the patients had often already developed stage III disease.

Our collection spanned several years, during which time therapies for advanced melanoma have evolved. Samples therefore reflect the standard of care and ongoing clinical trials at contributing centers, ranging from untreated to targeted therapy to immune checkpoint blockade to combination therapies (Figure 2E).

Genomic Characterization and Clinical Annotation

The majority (n = 314, 68%) of PDX and tissues were analyzed for genomic alterations using massively parallel sequencing of a 108-gene-targeted panel. Genes included in this panel were selected based on previously described mutations and copy number variations in melanoma. A full list of included genes and an in-depth analysis of mutational and copy number data of all PDX models as well as additional melanoma cell lines (n = 488 total) are provided in a companion resource article (Garman et al., 2017 [this issue of *Cell Reports*]). An additional 90 patients were annotated by NGS targeted panels of 40–400 genes at their clinical institutions, and we used these data to infer oncogenic driver mutation status of PDX. Both datasets were combined to classify a total of 372 PDX or banked tissues into major mutational subgroups.

Half (55%) of all analyzed samples were *BRAF* hotspot mutant, 20% *NRAS* mutant, 7% *NF1* mutant, 2% *KIT*, 1.4% *GNAQ*/*GNA11*, and 18% WT (Figure 3A; Data S2). These results correlate with the melanoma TCGA data (Cancer Genome Atlas, 2015) and other published large-scale sequencing studies (Arafeh et al., 2015; Hodis et al., 2012; Krauthammer et al., 2015).

Thirty-seven of the *BRAF* hotspot mutation PDX were from patients progressed on a BRAF inhibitor (12 previously published in

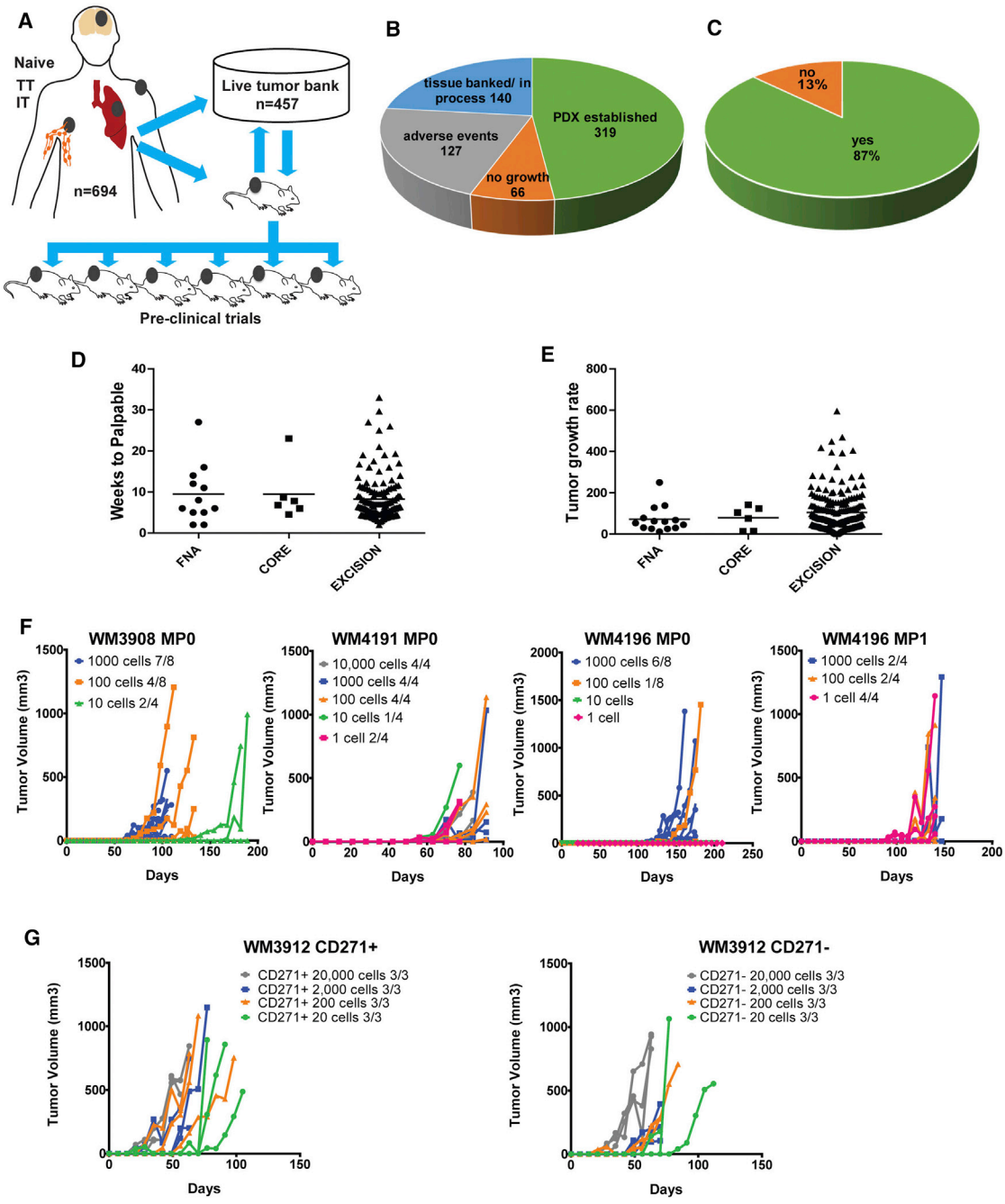

Figure 1. Establishment and Biology of PDX Models

(A) A total of 694 melanoma tissue samples from naive, pre-, on-, or post-therapy time points receiving targeted kinase inhibitors (TT) or immune checkpoint inhibitors (IT) were used to generate PDX and/or were banked as live tissue.

(B) Success rate of establishing a tumor graft (green), banking of live tissue with the potential of establishing a PDX or establishment in progress (blue), no tumor growth at 6 to 12 months (orange), and adverse events (gray), where we were not able to establish a PDX because of reasons other than tumor take (this analysis excludes uveal primary samples).

(C) Take rate of cutaneous melanoma-derived tissue.

(D) Time to palpable for all FNA, core, and excisional biopsy patient samples.

(E) Tumor growth rate comparison of FNA, core, and biopsies. Growth was calculated as tumor volume per weeks.

(F) Fresh tumor biopsies (MP0) or PDX after MP1 from three patients were prepared as cell suspensions (leucocytes and endothelial cells excluded) and injected s.c. into NSG mice at the indicated cell numbers.

(G) Single-cell suspension was prepared as before and sorted for CD271 marker. CD271+ and negative cells were injected at indicated cell numbers.

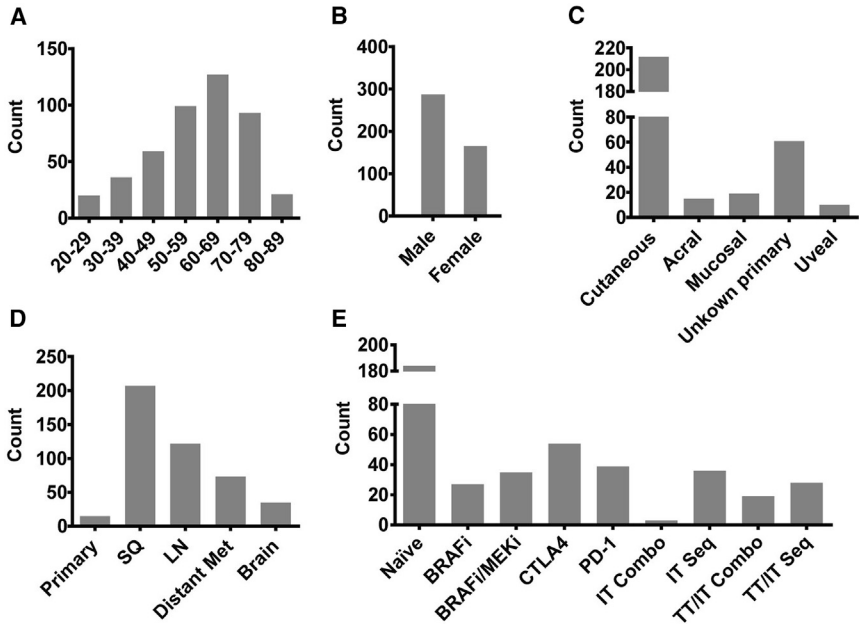

Figure 2. Demographics of Patient Samples Used to Generate PDX

(A) Age of patient at time of biopsy in 10-year increments.

(B) Gender of patient.

(C) Primary tumor type.

(D) Site of tissue biopsy categorized into primary melanoma, subcutaneous metastasis (SQ), lymph node (LN) metastasis, distant metastasis to organs (distant met), and brain metastasis (brain).

(E) Targeted kinase or immune checkpoint inhibitor therapies the patient had received before or during the biopsy. Samples without available data were excluded from the analysis.

Krepler et al. [2016]) and 44 progressed on BRAF/MEK inhibitor combination therapy. We collected 190 samples from patients with immune checkpoint inhibitor therapy (anti-CTLA4 and/or anti-PD-1). These did not cluster to any mutational subgroup. We established PDX from patients progressed on both targeted and immune therapy (25 sequentially and 17 with BRAF inhibitor/PD-1 blockade combination therapy) (Figure 3A; Data S2).

The reverse-phase protein array (RPPA) platform quantified ~300 proteins and phosphorylated proteins. These profiles are a useful complementary analysis to genetic sequencing (Krepler et al., 2016) and are available for 113 PDX models, while others are in progress (Figure 3A; Data S3).

PDX-Derived Cell Lines

We have established cell lines from 24 PDX tumors with a focus on targeted therapy resistant and brain metastasis samples (Figure 3A). These are added to the 112 cell lines of the "Wistar Melanoma" collection (https://www.wistar.org/lab/meenhard-herlyn-dvm-dsc/page/melanoma-cell-lines-0). As these PDX-derived cell lines included 10 derived from targeted therapy-resistant samples, the mutational distribution is biased for BRAF hotspot (71%). Further, the cell lines include 7 from brain metastasis, 2 acral melanoma (WM4324: V600E, WM4235: Q61R), and 1 mucosal (WM4173: WT/WT).

PDX from Patients Treated with Checkpoint Inhibitors

We established 190 PDX from 140 immune checkpoint blockade therapy patients. The best response was complete response in 7 patients, partial response in 26, mixed response in 5, stable disease in 10, and progressive disease in 59 patients. Response data could not be obtained in 33 patients. Forty-three patients received only anti-CTLA4, and 50 received only anti-PD-1; 41 patients received both therapies sequentially and 6 as a combination therapy. All patient samples were collected before, on-, or after immune therapy with 16 patients matched before and on or after therapy (Figure 3B).

PDX from Targeted Therapy-Resistant Patients

We collected 57 biopsies from 47 patients after progression on BRAF or BRAF and MEK combination targeted kinase inhibitor therapy (either still on or shortly after end of therapy) (Figure 3C). After initial establishment and expansion as PDX, the tumor-graft-bearing animals were continuously dosed with BRAF inhibitor (PLX4720) or BRAF/MEK inhibitor (PLX4720/PD-0325901) combination diet corresponding to the type of therapy received by the patient (Krepler et al., 2016). Targeted sequencing of resistant PDX tumors using our 108-gene panel (Garman et al., 2017) confirmed a BRAFV600 hotspot mutation in all but two of the models. These two PDX models were established from patients with clinical BRAFV600E-positive tumors. However, the patient material tested for WM4323 was the primary cutaneous melanoma diagnostic biopsy accessioned 5 years prior to the specimen sent for PDX. This was done via pyrosequencing of codons 595 and 600 of exon 15 of the BRAF gene. The patient material tested for WM4352 was a metastatic lymph node accessioned 7 months prior to the specimen sent for PDX. This was done via NGS panel of 50 genes including, for BRAF, codons 439–473 of exon 11, and codons 581–611 of exon 15.

Several mechanisms of resistance were revealed by targeted sequencing. We found concomitant *RAS* (n = 7/47 patients) and *MAP2K1/2* (n = 9/47 patients) mutations. These deleterious mutations were mutually exclusive and have been reported previously as activating mutations conferring resistance to BRAF inhibition (Emery et al., 2009; Nazarian et al., 2010). *BRAF* high-level amplification (>5) in 4 patients and *MET* high-level amplification (> 5) in 3 patients were exclusive of each other and *RAS*- and *MAP2K*-activating mutations (Shi et al., 2014). PDX from 15 patients had alterations in the PI3K signaling pathway (13 PTEN deletion, 3 deleterious PTEN mutation, 5 likely deleterious PTEN mutation, 1 deleterious PIK3CA mutation), although these were not mutually exclusive with the other genomic changes observed.

Patient-matched PDX from before start and after progression on targeted therapy were generated from 7 patients. Of these,

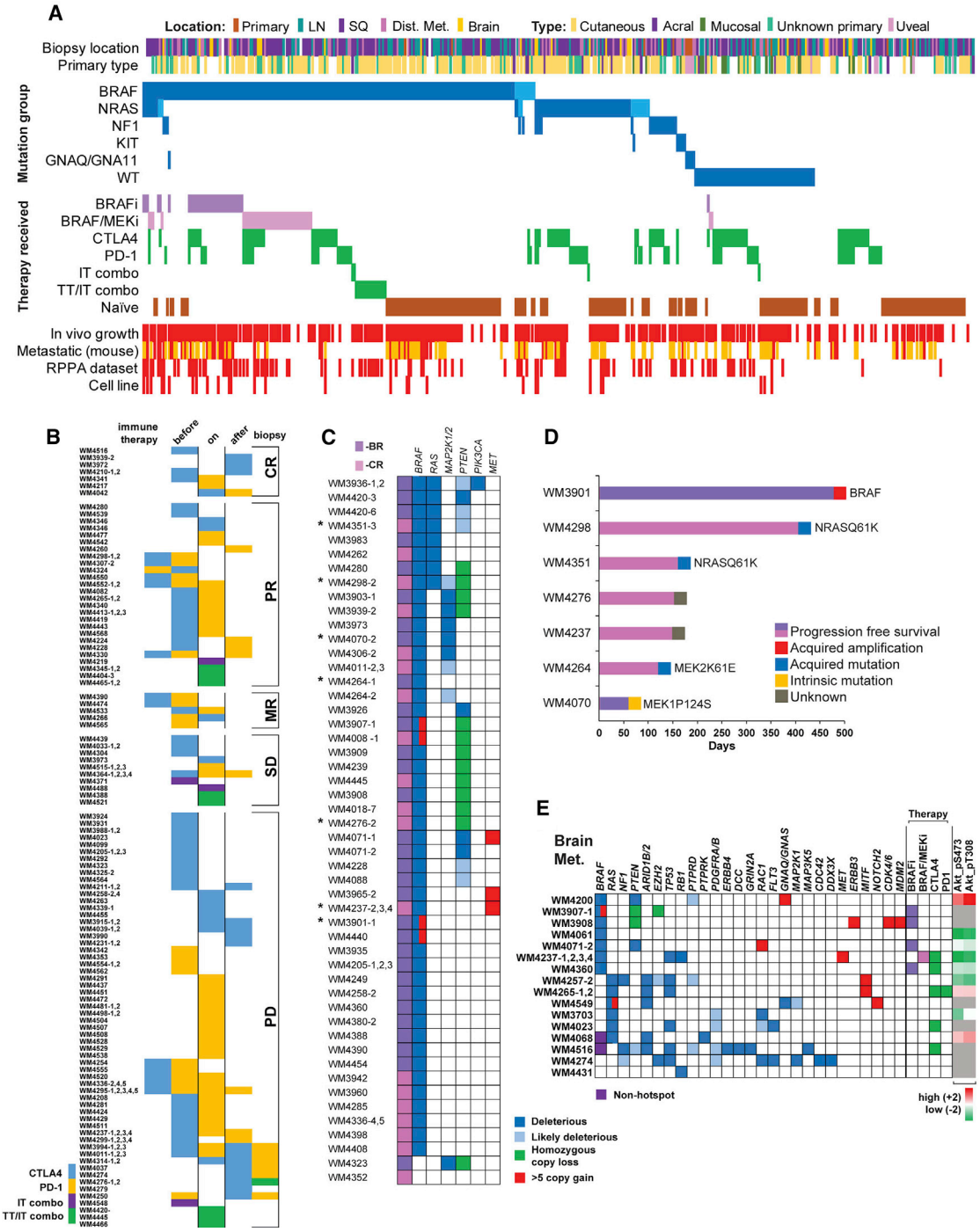

Figure 3. Overview of PDX Collection, Immune Therapy, Targeted-Therapy-Resistant Samples, and Brain-Metastasis-Derived Subsets

(A) All PDX and live frozen tissue samples sorted by driver mutations and therapy received by the patients. Driver mutations are dark blue for hotspot and light blue for non-hotspot mutations. PDX from patients progressed on targeted therapies are shades of purple; patients treated with immune checkpoint inhibitors are green: sequential, combination CTLA4+PD-1 (IT combo) or combination with BRAF inhibition (TT/IT combo). Red indicates *in vivo* growth, presence of RPPA data, or a corresponding cell line. Samples that spontaneously metastasize to lungs in mice are red; yellow indicates no lung metastasis; and white indicates not assessed.

(B) Patients were treated with CTLA4 or PD-1 blocking therapy before, during, or after biopsy. Combination therapies are indicated. PDX are sorted by best response in the patients. Additional PDX with unknown response are not shown.

(C) Genetic data of BRAF (−BR) and BRAF/MEK (−CR) inhibitor-resistant PDX. Deleterious and likely deleterious mutations, homozygous loss, and high copy number gains (>5) are shown. Numbering after dash (1–4) indicates additional PDX available from the same patient. Asterisks indicate resistant PDX with available patient-matched pre-therapy-derived PDX.

(legend continued on next page)

two (WM4298, WM4351) acquired NRAS mutations on dabrafenib/trametinib (D/T) combination therapy and progressed after 406 and 161 days, respectively. WM3901 was established from a solitary progressing (>10%) s.c. metastasis after 480 days on D/T combination therapy and had acquired a BRAF amplification. WM4264 had PFS of 120 days and an acquired MEK2K61E heterozygous mutation in the relapse PDX. Although a variant of unknown significance per our algorithm (Garman et al., 2017), because of the location and glutamic acid change, this might be a phosphomimetic-activating mutation (Villanueva et al., 2013). WM4070 PDX were established from the patient with the shortest PFS (60 days), and we found a pre-existing MEK1 mutation in both pre-and post-therapy PDX. The remaining two models (WM4276, WM4237) had pre-existing loss of PTEN and amplification of MET, respectively, as possible contributors to resistance (Figure 3C).

Protein Expression Profiles

RPPA was performed on a total of 118 PDX models in triplicate and divided between two batches. Set 102 (Data S3) had 184 profiles representing 60 models including one model with corresponding untreated and BRAF inhibitor treated samples. Set 119 (Data S4) had 243 profiles containing 58 models, 23 of which have corresponding untreated and BRAFi- and/or BRAFi/MEKi-treated tumor samples. Set 102 assessed 279 phospho- and total proteins, and set 119 assessed 299 phospho- and total proteins.

PDX Derived from Brain Metastasis

We collected melanoma brain metastasis (MBM) tissue from 34 neurosurgeries of 28 patients to generate PDX models. Targeted sequencing data are currently available for 20 PDX and RPPA data for 12 (Figure 3D). Remarkably, four brain metastases were collected from the same patient (WM4237-1 to -4) at 2- to 4-month intervals. Although the patient had received D/T combination therapy (best response, stable disease) after the first surgery, and had received anti PD-1 therapy during the last two surgeries, all four PDX had identical mutation profiles (BRAFV600E RB1N690fs TP53S241). PDX from 7 patients had BRAF hotspot mutation and from 6 patients NRAS hotspot mutation. One of these had a co-occurring BRAF non-hotspot mutation. Another BRAF non-hotspot mutation was co-occurring with an NF1 mutation. Two patients were WT for both BRAF and NRAS. Interestingly, the samples without BRAF hotspot mutation had significantly more concurrent deleterious and likely deleterious mutations overall. We found PTEN deletion or deleterious mutation in 4 of 7 patients with BRAF hotspot mutation which has been shown to be associated with MBM (Bucheit et al., 2014). On the protein expression level, both patients with deleterious PTEN mutations had evidence of PI3K pathway activation by relative increased phospho-AKT compared to WT PTEN samples.

PDX from Primary or Metastatic Uveal Melanoma Samples

We implanted 45 uveal primary samples as tumor fragments s.c. in the interscapular fat-pad of NSG mice with matrigel (Némati et al., 2010). After follow-up of at least 12 months, we observed tumor growth in five models, albeit kinetics were slow. Three of these had mutations in GNAQ or GNA11; one was WT; and one failed genomic analysis. In contrast, the take rate for metastatic samples from uveal melanoma patients was comparable to cutaneous melanoma, and we established four samples as PDX; one with a GNAQ mutation; and the others are in process.

Availability of PDX Models to the Research Community

A critical component of our PDX platform is its availability to the research community. Like cell line repositories, PDX tissue can be frozen and expanded as needed. Thus, we made a representative pre-selection of 26 "work horses" based on genetic and clinical criteria (https://www.horizondiscovery.com/patient-derived-xenograft/melanoma-pdx) (Data S2). All other models are available on request, and tissue will be expanded either at Horizon Discovery (St. Louis, MO, USA) or at our laboratory.

Spontaneous Metastasis Rate Is Associated with Mutational Group

When cells from a PDX model were inoculated into a human skin graft on NSG mice (Li et al., 2015), tumors formed within the human dermis. These then metastasized out of the human graft into the lungs of host mice as an indicator for distant organ metastasis (Figures 4A–4C). This propensity to invade the mouse tissue and seed distant organs was reflected in the subsequently observed high rates of spontaneous metastasis in s.c. implanted PDX models. We analyzed lungs of mice at the time of tumor harvest (Figure 4D) and found that in 32% of PDX models assessed, more than 80% of the animals had micro- or macro-metastases (Figure 4E). There was a significant increase in metastatic ability of *BRAF* hotspot mutant PDX and a decreased metastatic rate in triple WT PDX (Figure 4F).

Spontaneous Brain Metastasis Model

An MBM-derived PDX was established as a short-term culture, transfected with a luciferase reporter and implanted s.c. into NSG mice. To prolong survival of animals, primary tumor grafts were surgically removed once established (Figure 4G). We observed spontaneous metastasis to the mouse brain in 50% of animals after a latency of 120 days (Figure 4H). Additional models are in development.

PDX Tumors Resistant to MAPK Inhibitors Have Increased IGF1R Expression

We assessed expression of a panel of melanoma surface receptors previously described as cancer stem cell markers including

(D) Patient matched pre- and post-therapy PDX models. Progression-free survival of patients treated with BRAF or BRAF/MEK inhibitor (x axis). Columns are labeled with putative resistance mechanisms.

(E) Genetic profile and therapy received of 22 PDX with available sequencing data out of 31 total brain metastasis PDX. Deleterious and likely deleterious mutations, homozygous loss, and high copy number gains (>5) are shown. As an indication of PI3K pathway activation status, RPPA levels of phosphorylated AKT are shown.

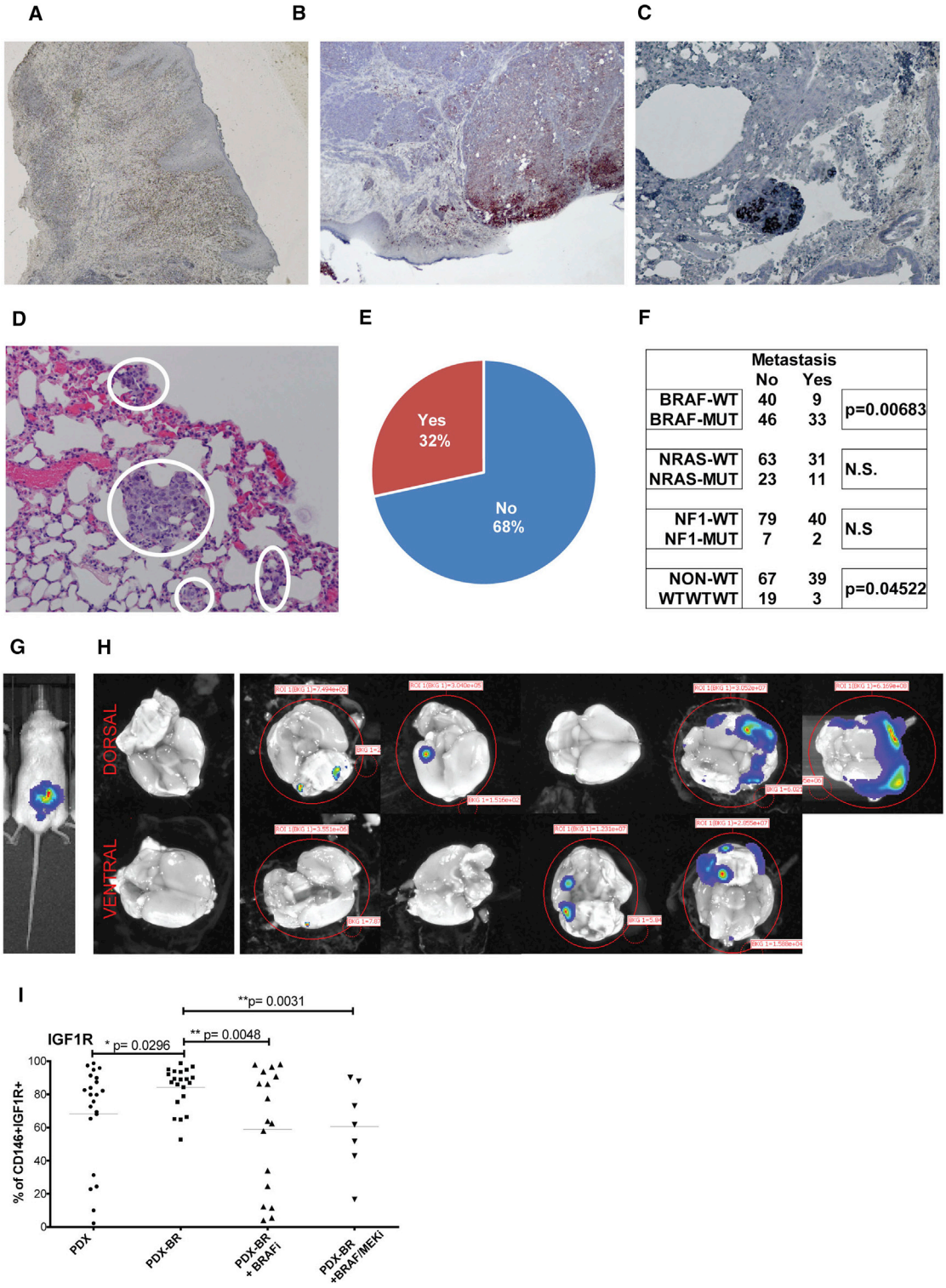

Figure 4. Melanoma PDX Metastasize Spontaneously

(A) Animals were grafted with neonatal foreskin grafts, and melanoma PDX cells were injected into established grafts.

(B) Melanoma lesions formed in the human skin reconstructs.

(C) Melanomas spontaneously metastasized to the mouse lungs from the human skin graft. H&E staining; representative images.

(D) Example of spontaneous micro-metastasis to lung.

(legend continued on next page)

CD20 (Fang et al., 2005), CD271 (Boiko et al., 2010), and CD133 (Monzani et al., 2007) in two cohorts of therapy naive and resistant PDX. There were no significant differences observed for any of the markers (data not shown). However, tumors derived from targeted-therapy-progressed patients had significantly higher levels of IGF-1R than tumors from therapy naive patients (Figure 4I). IGF-1R/PI3K signaling has previously been implicated in conferring melanoma resistance to BRAF inhibitors (Villanueva et al., 2010). Interestingly, when the resistant tumor grafts were grown on continuous BRAFi or BRAF/MEKi combination diet, the IGF-1R levels returned to baseline (Figure 4I). This phenomenon might indicate the transient nature of tyrosine kinase receptor upregulation and its modulation by MAPK pathway inhibitors.

Predictive Value of PDX for Response to Targeted Therapies

We selected a PDX from a 55-year-old female patient with metastatic melanoma and early relapse to vemurafenib after partial response using RECIST 1.1 criteria and progression-free survival of 16 weeks. Lymph node lesions in her right and left axillary regions showed initial on-treatment regression: there was a 70.6% decrease in the target lesion (i.e., the right axillary node) and a partial response in the non-target lesion (the left axillary node) (Figure 5A). An FNA was taken from the left lymph node before therapy and used to generate a PDX. After *in vivo* expansion, tumor-bearing animals were treated with the BRAF inhibitor PLX4720 alone and in combination with the MEK inhibitor PD-0325901. Tumors did not respond to BRAF inhibition, but regressed on BRAF/MEKi combination followed by relapse (Figure 5B). This was reflected in a reduced proliferation rate in the combination therapy tumor cells only (Figure 5C).

MEK and PI3K Beta Inhibition as Second-Line Therapy in BRAF-Inhibitor-Resistant Models

We selected three *BRAF-V600E* PDX models derived from patients relapsed on BRAF inhibitor. Two had homozygous PTEN deletion, and one had an activating NRASQ61K mutation; all showed activation of both MAPK and PI3K pathways on the protein level (Krepler et al., 2016). The MEK inhibitor trametinib and the PI3K beta/delta isoform-specific inhibitor GSK418 (an analog of GSK2636771 (R.A. Rivero and M.A. Hardwicke, 2014, Cancer Res., abstract) significantly decreased tumor growth in the two PDX models with PTEN deletion without evident toxicity (Figure 5D), but not in the PDX with concurrent BRAF and NRAS mutation.

ERK and MDM2 Inhibition Is Highly Effective in a BRAF-Inhibitor-Resistant PDX Model

WM3973 was derived from a patient progressed on vemurafenib with MAPK pathway reactivation via an activating *MAP2K1* (MEK1) mutation as a potential resistance mechanism (Krepler et al., 2016). Accordingly, this PDX model did not respond to BRAF inhibition or even to the downstream targeting ERK inhibitor BVD-523. We then applied a previously published response biomarker signature for p53 reactivation (Jeay et al., 2015) to a cohort of 9 *TP53* WT BRAF-inhibitor-resistant PDX models. The majority, including WM3973, were predicted to be sensitive to MDM2 inhibition (data not shown). The MDM2 inhibitor CGM097 (Holzer et al., 2015) moderately inhibited WM3973 tumor growth as a single agent, but ERK and MDM2 inhibition synergized potently to induce stable disease over 6 weeks of dosing (Figure 5E, left panel).

Typical of the tumor growth heterogeneity seen in PDX experiments, single mice showed a variable response to the combination therapy (Figure 5E, right panel). Whereas tumors in most animals had stable disease, two tumors showed early relapse, and two tumors had complete responses at the end of dosing. Both regrew only after treatment was stopped, confirming that in PDX models small residual tumors can survive following several weeks of drug therapy. However, we did not observe any tumors acquiring resistance while on combination therapy, indicating that this approach could be explored further using additional models.

We analyzed protein expression profiles of tumor grafts at the end of dosing to investigate the heterogenous responses seen with this therapy. The clusters from unsupervised hierarchical clustering identified groups that were predominately based on proteins with a role in proliferation and correlated with tumor growth rates rather than dosing groups (Figure S1). The BVD-523 single-agent group whose tumors grew at the same rate as controls, clustered with the fastest growing tumors in the control group, indicating that ERK inhibition alone did not widely change the protein and phosphoprotein levels assessed in this array. Indeed, there was no inhibition of pERK on RPPA. However, the BVD-523 single-agent group had the least tumor growth variability with all tumors progressing rapidly. All tumors with continued response to combination treatment clustered in one group, whereas the two tumors with early resistance to the combination therapy clustered with the CGM single-agent samples.

Rapid *In Vivo* Screen for BET Inhibitor Activity in a Broad PDX Panel

We used the novel BRD4 inhibitor BAY8097 to conduct a rapid *in vivo* screen on 20 PDX of diverse mutational profiles. To test feasibility, we reduced group size from 10 to 3 mice per group. Like the model in Figure 3E, we observed significant heterogeneity in tumor growth, a problem also encountered in a recently published study using only one tumor graft/PDX/therapy (Gao et al., 2015). We found that a subset of models not clustering into a mutational subgroup showed significant tumor growth inhibition using BAY8097 as a single agent (Figure 5G).

(E) Percentage of PDX that metastasize to lungs in more than 80% of animals from the s.c. tumor graft at the time point of maximal tumor volume.
(F) Number of PDX with spontaneous lung metastasis compared to main mutational subgroups.
(G) Luciferase-transfected brain metastasis PDX injected s.c.
(H) Spontaneous metastases to the mouse brain were imaged ex vivo after a latency of 120 days after survival surgery.
(I) Percentage of IGF1R-positive cells in PDX from naive patients, from patients progressed on BRAF inhibitor (−BR), from patients on BRAF inhibitor, or from patients on BRAF/MEKi combination diet.

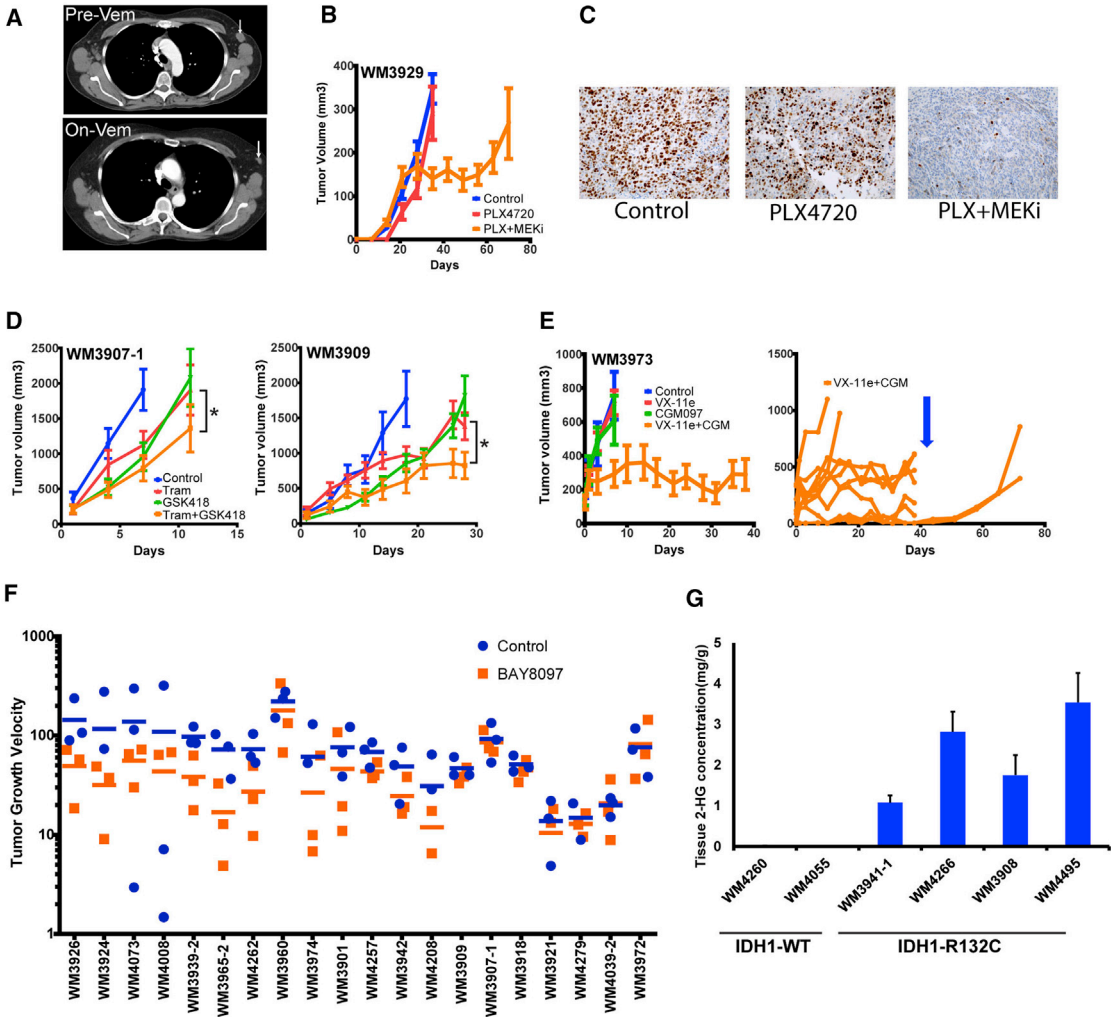

Figure 5. PDX Models in Pre-clinical Trials

(A) Computed tomography scans of patient with early relapse on vemurafenib and whose tumor was used to generate a PDX from a pre-therapy LN metastasis. Arrow indicates the lymph node metastasis biopsied, imaged before and 3 months on vemurafenib therapy.

(B) The PDX-bearing mice were fed a chemical additive diet containing PLX4720 200 ppm as single agent or in combination with PD-0325901 7 ppm (PLX+MEKi). The combination diet inhibited the PDX tumors' growth, followed by early on-therapy relapse.

(C) Ki67 staining indicating actively proliferating cells from tumor grafts on indicated treatments.

(D) Two PDX models from patients relapsed on BRAF inhibition (n = 10/group) were treated with chemical addictive diet containing the MEK inhibitor trametinib 2.1 ppm (Tram), the PI3K beta inhibitor GSK231418 214.3 ppm (GSK418), or the combination of both. An asterisk indicates the combination significantly inhibited tumor growth over single agents in both models.

(E) PDX model from a *BRAF-V600E* patient relapsed on vemurafenib (PFS 46 weeks, best response stable disease) that had an additional activating *MEK* mutation, *TP53* WT, and a biomarker signature indicating sensitivity to p53 reactivation. PDX tumors (n = 10/ group) were treated with the ERK inhibitor BVD-523 50 mg/kg twice daily oral gavage, the MDM2 inhibitor CGM097 100 mg/kg once daily oral gavage, or the combination of both. (Right panel) Single mouse growth curves of the BVD-523 + CGM-treated group highlighting the heterogeneity of response in PDX models. While most tumors showed stable disease, two mice had early relapse and two mice had complete responses (CR). Dosing was stopped on day 38 (blue arrow), and the 2 CR mice showed regrowth of residual disease.

(F) 20 PDX of *BRAFV600* mutant patients (naive and BRAF inhibitor resistant), *NRAS* mutant, and *BRAF-WT NRAS-WT* (n = 5 models each) were treated with the BET inhibitor BAY8097 10 mg/kg once daily by oral gavage (orange) or vehicle control (n = 3/group, blue) in a rapid *in vivo* screen. Although variability within the PDX models was high, tumor growth velocity was decreased in a subset of models. Response was independent of mutation status.

(G) *IDH1* mutant PDX have increased 2-HG onco-metabolite levels in tumor tissue compared to *IDH1* WT PDX.

Validation of Increased Onco-Metabolites in PDX with IDH1 Mutation

We identified 8 PDX with the canonical *IDH1* mutation R132C. Only one melanoma cell line with very slow growth kinetics has been described in the literature (Lopez et al., 2010). Indeed, we were unsuccessful in establishing cell lines from these patient samples (data not shown). We tested levels of the D-2-hydroxyglutarate (2-HG) onco-metabolite (Mondesir et al., 2016) and confirmed buildup to very high levels as compared to WT in PDX tissue (Figure 5H).

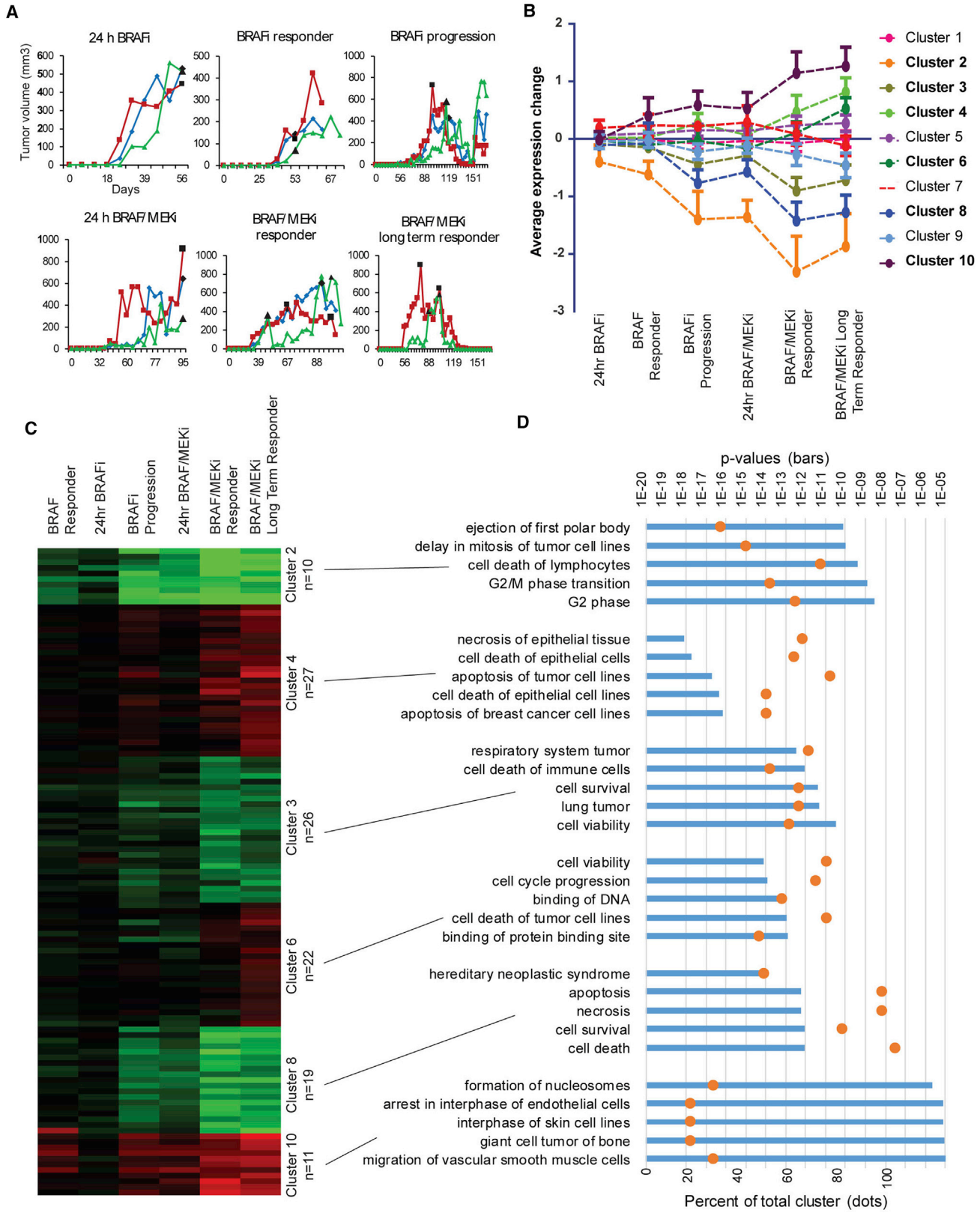

(legend on next page)

PDX Can Model Pathway Adaptation to Targeted Drugs over Time

To assess the potential of PDX models to mimic acquired drug resistance, we performed a time-course analysis of response and acquired resistance to a BRAF inhibitor in a targeted therapy-naive *BRAF-V600E* PDX. The patient had received BRAF inhibitor therapy after the biopsy was taken and initially responded followed by relapse after 9 months. Although, the patient never received BRAF/MEK combination therapy, we followed up with this combination in our PDX model (Figure 6A). The PDX tumors initially responded to BRAF inhibition with almost complete tumor regression but relapsed 7 seven weeks; however, when the same animals were switched over to BRAF/MEK inhibitor combination, they again responded continuously without relapse for up to 2.5 months. Tumors from each treatment were analyzed for protein expression by RPPA in a time-course manner (Figure 6B; full dataset in Data S5). Protein expression only changed significantly with the onset of BRAF inhibitor resistance (Figure 6C), and the subsequent change to BRAF/MEK inhibitor combination therapy shut down cell proliferation, induced apoptosis, and led to sustained tumor growth inhibition (Figure 6D). Thus, PDX models can be used to track changes in tumor cell signaling on the protein level over the course of therapy.

DISCUSSION

Established melanoma cell lines have significant bias toward BRAF, TP53 mutations, and CDKN2A loss (Garman et al., 2017) since these adapt well to in vitro growth. The much higher success rate of PDX regardless of mutational subgroup make PDX more clinically relevant (Byrne et al., 2017; Townsend et al., 2016). Several other research groups have established melanoma PDX models (Einarsdottir et al., 2014; Gao et al., 2015; Girotti et al., 2016; Kemper et al., 2016; Quintana et al., 2012). Quintana et al. (2012) established PDX from 25 stage IIIB/C patients and correlated spontaneous metastasis in the animals with patient outcome. Einarsdottir et al. (2014) established PDX from 23 patients and predicted targeted therapy responses in a subset. Gao et al. (2015) employed a 1 × 1 × 1 *in vivo* trial design in 277 PDX including 67 melanoma derived, demonstrating clinical translatability of this approach. Kemper et al. (2016) established 89 PDX, but focused on BRAF mutant patients with only 10 NRAS and 6 WT/WT samples. They then used this platform to identify a novel resistance mechanism to BRAF inhibition in the form of a duplicated kinase domain. Girotti et al. (2016) have built a collection of about 90 PDX models, of which they show 3 deeply characterized examples by following the development of resistance to targeted therapy over time using whole-exome sequencing. Together, these studies show the promise and potential of PDX models in melanoma.

Multiple resistance mechanisms to targeted therapy have been described and these most often lead to reactivation of the MAPK pathway or activation of alternative pathways such as the PI3K signaling pathway (Rizos et al., 2014). Pre-clinical data by several groups have suggested that combining BRAF/MEK inhibitors with PI3K/mTOR inhibitors may overcome resistance in *BRAF* mutant melanomas (Atefi et al., 2011; Greger et al., 2012; Shannan et al., 2016; Villanueva et al., 2010). Phase I clinical trials using this combination demonstrated the safety of this combination approach and some early signs of clinical activity (Bedard et al., 2015; D. Juric et al., 2014, J. Clin. Oncol., abstract), and further phase I/II trials are ongoing (NCT01449058; https://clinicaltrials.gov). On the other hand, a phase I trial testing the combination of pan-PI3K/mTORC1/2 inhibitor GSK2126458 with trametinib was terminated due to a lack of tolerability and efficacy (NCT01248858), suggesting a narrower targeting profile might be advantageous. Thus, our pre-clinical PDX trial confirmed that combination of a beta isoform specific PI3K inhibitor retained synergistic potential with MEK inhibition but could potentially decrease toxicity.

We included PDX with diverse mutational backgrounds that were either naive or progressed on targeted therapy in an *in vivo* screen of a novel BET inhibitor. Targeting the transcriptional activity of cancer cells has emerged recently as a novel strategy (Filippakopoulos et al., 2010). It is unclear however, which patients would benefit from these inhibitors and whether it would be a viable strategy in a clinical setting for melanoma (Segura et al., 2013). Our PDX collection is large enough to mirror the diversity of patients that would be studied in an early-stage clinical trial at a fraction of the cost and could be beneficial for early-stage drug screening as well as for the development of biomarkers. The activity of BET inhibition seen in a subset of PDX models, although hampered by high heterogeneity, still warrants further investigation into this class of compounds and use of the PDX data to identify response biomarkers.

Another strength of our large collection of PDX is the breadth of coverage including multiple samples with rare mutations, made possible by large-scale targeted sequencing of PDX (Garman et al., 2017). *IDH1* is a rarely mutated oncogene in melanoma, representing about 6% of driver mutations (Cancer Genome Atlas, 2015) and has been described as a viable target in other cancers (Tateishi et al., 2015). Since PDX are a living resource, we could functionally validate the mutation by assessing the accumulation of the onco-metabolite 2-HG in the tumor grafts. Thus, these models would be ideal to test inhibitors of IDH1.

MBM is a common event in late-stage patients and has a poor prognosis of less than one-year median survival (Staudt et al., 2010) even with modern systemic therapies (Forschner et al., 2017). Although current targeted and immune therapies have

Figure 6. Protein Pathway Activation over Time and in Response to MAPK Inhibition

(A–D) WM4007 was generated from a pre-BRAF inhibitor therapy biopsy. (A) PDX growth curves for mice treated with PLX4720 (BRAFi) or PLX4720+PD-0325901 (BRAF/MEKi) diet started at time points indicated by black data points. (B) Protein expression change patterns identified in RPPA data with K means clustering. All proteins within each cluster are averaged, and SD is shown. Clusters in bold had variation above 0.1 and were analyzed further. (C) Hierarchical clustering of RPPA data normalized to controls depicting the significant K means clusters along each time point. (D) Ingenuity pathway analysis (IPA) was used to assign proteins within each cluster into distinct biological processes. (Top axis) The top five significant gene ontology terms within each cluster are displayed with bars. (Bottom axis) The percentage of each cluster's proteins found within each biological functional category is displayed with orange dots.

demonstrated activity in MBM, successful therapy is still a major challenge and an important area of current investigation (Glitza Oliva et al., 2017). MBM models are scarce and new therapies are needed urgently. Thus, we focused our collection efforts on samples derived from MBM, and these will provide a valuable resource to study this challenging to treat and frequently lethal manifestation of late-stage melanoma.

Although patients can show long-lasting responses to immune checkpoint blockade, many patients do not respond or acquire resistance. Clinical studies point toward the importance of the immune infiltrate in tumors (Chen et al., 2016); however, human tumor-infiltrating lymphocytes implanted with the initial patient tumor tissue are lost in PDX propagation. High mutational load is associated with increased response rates to immune therapies with neo-antigens the target of immune responses (Peng et al., 2016). Thus, PDX models from checkpoint inhibitor responders and non-responders could potentially be valuable tools to study the role of tumor biology in response to immune therapy, and we are currently investigating neo-antigens. Our collection of PDX can be used to study checkpoint inhibitors or other immune therapies alone or in combination with targeted kinase inhibitors when employed in humanized mouse models (unpublished data). In these models, human CD34+ hematopoietic stem cells are injected to reconstitute human B and T cells in NSG mice (Rongvaux et al., 2014). Thus, the current limitations of model could potentially be addressed using humanized mice and would allow PDX models to be at the forefront of immune and targeted therapy translational research (Sanmamed et al., 2016). These studies are ongoing.

In summary, we have built a unique and comprehensive melanoma PDX collection representing the entire spectrum of this cancer with multiple biological replicates even for rare subgroups. It is further enhanced through genetic and genomic analysis in our companion paper (Garman et al., 2017).

EXPERIMENTAL PROCEDURES

Detailed SOPs for all aspects of PDX generation and use are provided in Data S1.

Patient Sample Processing

Patient samples were collected under institutional review board (IRB) approval. Tumor samples were processed within 24 hr of biopsy. Samples were mechanically dissociated and enzymatically digested if necessary. Tumor tissue was frozen in 10% DMSO and 90% fetal bovine serum (FBS), if sufficient quantities were available, or implanted directly into NSG mice. Mice were anesthetized; a small skin incision (~5 mm) was made in the back of the animal; and an s.c. pocket was created. Tumor fragments were implanted with 100 μL of matrigel, and the incision was closed with a wound clip.

PDX Maintenance

All animal experiments were performed in accordance with institutional guidelines under Wistar IACUC approval. PDX were expanded in NSG mice. Tumor size was assessed once weekly by caliper measurements ([length × width^2]/2). Animals were sacrificed when the tumors reached 1,000 mm^3 or when necessary for animal welfare. The larger part of the tumor was retained as a live tumor bank, the smaller part was reimplanted at a 1:5 ratio. PDX tumors from patients progressed on BRAF or BRAF/MEK inhibitor therapy were expanded on continuous PLX4720 200 ppm or PLX4720 200 ppm + PD-0325901 7 ppm chemical additive diet (Research Diets, New Brunswick, NJ, USA).

Pre-clinical *In Vivo* Trials

When tumors reached 200 mm^3, mice were randomized into treatment groups. 10 animals were assigned to each group in the efficacy studies to account for variability among tumors, except for the BAY8097 rapid *in vivo* screen, which was designed with three animals per group. Tumor size was assessed twice weekly per caliper measurement, and tumor volume was estimated using the formula ([length × width × width]/2). Mice were sacrificed after 2–3 weeks of treatment. If therapy groups showed tumor regression, dosing was prolonged.

Short Tandem Repeat Profiling

We performed short tandem repeat (STR) profiling on one tumor per mouse passage (MP) using the AmpFlSTR Identifiler PCR Amplification Kit (Life Technologies, Carlsbad, CA, USA), which uses loci consistent with all major worldwide STR standards. Genomic DNA was extracted from patient or xenograft tumor samples using the DNeasy Blood and Tissue Kit (QIAGEN, Valencia, CA, USA) in accordance with the manufacturer's instructions. PCR amplification and STR allele separation and sizing were performed by the Wistar Genomics Facility. Profile interpretation was performed in our lab by matching the resultant DNA fingerprint to our internal database, which includes over 1,000 fingerprints and is available on our website (https://www.wistar.org/lab/meenhard-herlyn-dvm-dsc/page/melanoma-cell-str-profiles). DNA fingerprinting was matched to normal blood DNA, if available, to confirm the identity of the samples.

Massively Parallel Sequencing

DNA from patients and/or PDX were characterized by massively parallel sequencing using a custom-designed 108-gene targeted panel. Results were annotated for mutations, insertions and deletions, and copy number changes. A detailed description of the methodology and analysis is provided in Garman et al. (2017). Briefly, DNA was purified (DNeasy Blood & Tissue Kit); 500 ng of genomic DNA was sheared randomly into 200-bp fragments; and sheared DNA was A-tailed and ligated with adaptor-embedded indexes using the NEBNext UltraTM DNA Library Prep Kit for Illumina (New England BioLabs, Ipswich, MA, USA). Samples were equimolarly pooled prior to capture with a 2.2 Mbp SureSelectXT Custom Target Enrichment Kit (Agilent Technologies, Santa Clara, CA, USA) targeting 108 genes previously implicated in melanomagenesis. Paired-end (2 × 100 bp) sequencing was performed on the HiSeqTM 2000 Sequencing System (Illumina, San Diego, CA, USA).

To account for mouse DNA contamination, previously unreported variants with an allelic fraction of less than 0.15 were filtered out of the analysis.

Foreskin Grafting Procedure

Prepared rectangles of about 1.5 × 2 cm foreskin were placed on skin defects on the back of a mouse with the *panniculus canosum* remaining intact. The *panniculus canosum* was needed to help vascularize the graft. The foreskin graft was then secured *in situ* using Tegaderm (3M, St. Paul, MN, USA). After 10 days, the dressing was removed, and the graft was fully healed in 5–6 weeks.

Immunohistochemistry

Formalin-fixed, paraffin-embedded tissue sections of xenograft tumors were cut into 4-μm sections, deparaffinized in xylene, rinsed in ethanol, and rehydrated. Then the tissues were stained with the Ki-67 mouse clone MiB-1 (Dako, Carpinteria, CA, USA; catalog no. M7240).

Flow Cytometry Staining

Tumors were analyzed after mechanical dissociation followed by filtration and red blood cell lysis. For surface staining, cells were incubated at 4°C for 30 min with anti-human PeCy7 CD146 (M-CAM), anti-mouse FITC- CD45, H2Kb, and H2Kd, and anti-human PE IGFR1 from BD Biosciences (San Jose, CA). Staining was performed in the presence of LIVE/DEAD Fixable Dead Cell Stains (Life Technologies). After dead cells and mouse cell exclusion, the percentages of double-positive CD146 and IGF1R cells were reported.

RPPA

The samples were prepared as previously described (Krepler et al., 2016). RPPA was performed by the MD Anderson Center RPPA core facility (Houston,

TX, USA) as previously described (Tibes et al., 2006). Unsupervised hierarchical clustering using centered correlation and complete linkage was performed on normalized log2 median-centered protein values using Cluster (v.3.0) software (http://bonsai.hgc.jp/~mdehoon/software/cluster/software.htm#ctv). Results were visualized using Java TreeView (v.3.0) software (http://jtreeview.sourceforge.net).

For WM4007 time-course analysis, normalized log2 values were median centered to the average of the untreated controls. The three tumors from each time point were averaged. K means clustering using Euclidean distance measure on 10 clusters (identified in unsupervised hierarchical clustering) run for 100 iterations was performed using Cluster (v.3.0) and visualized with Java TreeView. Clusters with variance greater than 0.10 across the time points were selected for gene ontology analysis using ingenuity pathway analysis (QIAGEN) for biological processes.

Statistical Analysis

The scatterplots with mean of multiple mice's tumor growth rates were reported by FNA, core, and excisional biopsy patient samples or by patient's sample. Shapiro normality tests were used to examine the distribution of studied variables. Non-parametric Mann-Whitney tests were used for between specific gene mutant group comparison. Linear mixed-effects models were used to test the difference of the tumor growth trends among treatment groups.

SUPPLEMENTAL INFORMATION

Supplemental Information includes one figure and five data files and can be found with this article online at https://doi.org/10.1016/j.celrep.2017.10.021.

AUTHOR CONTRIBUTIONS

C.K., K.S., M.B., M.X., B.S., A. Watters, and A.V. participated in PDX establishment, expansion, banking, and *in vivo* experiments. M.P. performed and analyzed flow cytometry experiments. G.Z. performed and analyzed IHC staining of tumor grafts. P.B. developed, performed, and analyzed quality control procedures. P.B. analyzed RPPA data. K.S. and C.K. developed experimental procedures. X.Y. and Q.L. performed statistical analysis. B.G., I.N.A., B.W., M.A.W., and K.L.N. developed, performed, and analyzed targeted sequencing. W.X., G.K., M.F., X.X., R.A., T.C.G., D.E.E., D.A.T., L.S., L.E.H., J.A.W., M.A.D., Y.L., G.B.M., D.T.F., M.B.-R., K.T.F., D.S.H., M.G., J.J.B., N.J.P., C.L.S., T.S., A.A., M.T., R.W.R., and A.R. performed tissue and clinical data collection. D.D., S.A., R.K., E.H., G.C., S.J., J.W., A. Walter, M.O., and M.B.B. participated in planning of *in vivo* experiments and data analysis. C.K., K.L.N., L.S., and M.H. participated in conception and design of the project. C.K., P.B., and M.H. wrote the manuscript. C.K. and M.H. supervised the work.

ACKNOWLEDGMENTS

We thank the animal, genomics, histology, flow cytometry, and imaging core facilities at the Wistar Institute. We thank the Perelman School of Medicine Biobank, University of Pennsylvania (Federico Valdivieso, Caitlin Feltcher, Amber McKeown, and Emma Gasper) with support from the Perelman School of Medicine and Abramson Cancer Center (P30 CA016520-40). We thank Lori E. Huelsenbeck-Dill and Patricia L. Swanson at the Helen F. Graham Cancer Center. We thank the tissue collection core facilities at the MD Anderson Cancer Center, Massachusetts General Hospital, and John Wayne Cancer Institute. We thank Drew A. Torigian for CT image analysis. We thank G. Bollag at Plexxikon for supplying PLX4720.

Support for the shared resources utilized in this study was provided by a Cancer Center Support Grant (CCSG) (P30CA010815) to the Wistar Institute, a Cancer Center Support Grant (CCSG) (CA016672) to MDACC, and the MDACC Melanoma SPORE (P50 CA093459). This work was supported by NIH grants (P01 CA114046, P01 CA025874, and R01 CA047159 to M.H.; R01 CA182635 to A.E.A.; R01 CA198015 and 5P30 CA016520 to R.A.); a SPORE grant on Skin Cancer to the Wistar Institute and the University of Pennsylvania (P50 CA174523-02); the Margaretta and R.R.M Carpenter Foundation; the SR Cancer Stem Cell Research Program (to the Helen F. Graham Cancer Center at Christiana Care); the University of North Carolina Cancer Research Fund (to D.D.); philanthropic contributions to The University of Texas MD Anderson Cancer Center Melanoma Moon Shot Program; and the Dr. Miriam and Sheldon G. Adelson Medical Research Foundation. The content is solely the responsibility of the authors and does not necessarily represent the official views of the NIH. This work was supported in part by grants from GSK, Novartis, and Bayer.

Received: September 27, 2016
Revised: August 18, 2017
Accepted: October 4, 2017
Published: November 14, 2017

REFERENCES

Alexandrov, L.B., Nik-Zainal, S., Wedge, D.C., Aparicio, S.A., Behjati, S., Biankin, A.V., Bignell, G.R., Bolli, N., Borg, A., Børresen-Dale, A.L., et al.; Australian Pancreatic Cancer Genome Initiative; ICGC Breast Cancer Consortium; ICGC MMML-Seq Consortium; ICGC PedBrain (2013). Signatures of mutational processes in human cancer. Nature *500*, 415–421.

Arafeh, R., Qutob, N., Emmanuel, R., Keren-Paz, A., Madore, J., Elkahloun, A., Wilmott, J.S., Gartner, J.J., Di Pizio, A., Winograd-Katz, S., et al. (2015). Recurrent inactivating RASA2 mutations in melanoma. Nat. Genet. *47*, 1408–1410.

Atefi, M., von Euw, E., Attar, N., Ng, C., Chu, C., Guo, D., Nazarian, R., Chmielowski, B., Glaspy, J.A., Comin-Anduix, B., et al. (2011). Reversing melanoma cross-resistance to BRAF and MEK inhibitors by co-targeting the AKT/mTOR pathway. PLoS ONE *6*, e28973.

Bedard, P., Tabernero, J., Januk, F., Wainberg, Z.A., Paz-Ares, L., Vansteenkiste, J., Van Cutsem, E., Perez-Garcia, J.M., Stathis, A., Britten, C.D., et al. (2015). A phase Ib, open-label, multicenter, dose-escalation study of the oral pan-PI3K inhibitor (BKM120) in combination with the oral MEK1/2 inhibitor (GSK1120212) in patients with selected advanced solid tumors. Clin. Cancer Res. *21*, 730–738, Published online December 10, 2014.

Boiko, A.D., Razorenova, O.V., van de Rijn, M., Swetter, S.M., Johnson, D.L., Ly, D.P., Butler, P.D., Yang, G.P., Joshua, B., Kaplan, M.J., et al. (2010). Human melanoma-initiating cells express neural crest nerve growth factor receptor CD271. Nature *466*, 133–137.

Bucheit, A.D., Chen, G., Siroy, A., Tetzlaff, M., Broaddus, R., Milton, D., Fox, P., Bassett, R., Hwu, P., Gershenwald, J.E., et al. (2014). Complete loss of PTEN protein expression correlates with shorter time to brain metastasis and survival in stage IIIB/C melanoma patients with BRAFV600 mutations. Clin. Cancer Res. *20*, 5527–5536.

Byrne, A.T., Alférez, D.G., Amant, F., Annibali, D., Arribas, J., Biankin, A.V., Bruna, A., Budinská, E., Caldas, C., Chang, D.K., et al. (2017). Interrogating open issues in cancer precision medicine with patient-derived xenografts. Nat. Rev. Cancer *17*, 254–268.

Callahan, M.K., Postow, M.A., and Wolchok, J.D. (2016). Targeting T cell co-receptors for cancer therapy. Immunity *44*, 1069–1078.

Cancer Genome Atlas, N.; Cancer Genome Atlas Network (2015). Genomic classification of cutaneous melanoma. Cell *161*, 1681–1696.

Chen, P.L., Roh, W., Reuben, A., Cooper, Z.A., Spencer, C.N., Prieto, P.A., Miller, J.P., Bassett, R.L., Gopalakrishnan, V., Wani, K., et al. (2016). Analysis of immune signatures in longitudinal tumor samples yields insight into biomarkers of response and mechanisms of resistance to immune checkpoint blockade. Cancer Discov. *6*, 827–837.

Einarsdottir, B.O., Bagge, R.O., Bhadury, J., Jespersen, H., Mattsson, J., Nilsson, L.M., Truvé, K., López, M.D., Naredi, P., Nilsson, O., et al. (2014). Melanoma patient-derived xenografts accurately model the disease and develop fast enough to guide treatment decisions. Oncotarget *5*, 9609–9618.

Emery, C.M., Vijayendran, K.G., Zipser, M.C., Sawyer, A.M., Niu, L., Kim, J.J., Hatton, C., Chopra, R., Oberholzer, P.A., Karpova, M.B., et al. (2009). MEK1

mutations confer resistance to MEK and B-RAF inhibition. Proc. Natl. Acad. Sci. USA *106*, 20411–20416.

Fang, D., Nguyen, T.K., Leishear, K., Finko, R., Kulp, A.N., Hotz, S., Van Belle, P.A., Xu, X., Elder, D.E., and Herlyn, M. (2005). A tumorigenic subpopulation with stem cell properties in melanomas. Cancer Res. *65*, 9328–9337.

Filippakopoulos, P., Qi, J., Picaud, S., Shen, Y., Smith, W.B., Fedorov, O., Morse, E.M., Keates, T., Hickman, T.T., Felletar, I., et al. (2010). Selective inhibition of BET bromodomains. Nature *468*, 1067–1073.

Forschner, A., Eichner, F., Amaral, T., Keim, U., Garbe, C., and Eigentler, T.K. (2017). Improvement of overall survival in stage IV melanoma patients during 2011-2014: analysis of real-world data in 441 patients of the German Central Malignant Melanoma Registry (CMMR). J. Cancer Res. Clin. Oncol. *143*, 533–540.

Furney, S.J., Turajlic, S., Stamp, G., Thomas, J.M., Hayes, A., Strauss, D., Gavrielides, M., Xing, W., Gore, M., Larkin, J., and Marais, R. (2014). The mutational burden of acral melanoma revealed by whole-genome sequencing and comparative analysis. Pigment Cell Melanoma Res. *27*, 835–838.

Gao, H., Korn, J.M., Ferretti, S., Monahan, J.E., Wang, Y., Singh, M., Zhang, C., Schnell, C., Yang, G., Zhang, Y., et al. (2015). High-throughput screening using patient-derived tumor xenografts to predict clinical trial drug response. Nat. Med. *21*, 1318–1325.

Garman, B., Anastopoulos, I.A., Krepler, C., Sproesser, K., Brafford, P., Wilson, M., Wubbenhorst, B., Amaravadi, R., Bennett, J., Beqiri, M., et al. (2017). Genetic and genomic characterization of 462 melanoma patient-derived xenografts, tumor biopsies and cell lines. Cell Reports *21*, this issue, 1936–1952.

Geller, A.C., Miller, D.R., Annas, G.D., Demierre, M.F., Gilchrest, B.A., and Koh, H.K. (2002). Melanoma incidence and mortality among US whites, 1969-1999. JAMA *288*, 1719–1720.

Girotti, M.R., Gremel, G., Lee, R., Galvani, E., Rothwell, D., Viros, A., Mandal, A.K., Lim, K.H., Saturno, G., Furney, S.J., et al. (2016). Application of sequencing, liquid biopsies, and patient-derived xenografts for personalized medicine in melanoma. Cancer Discov. *6*, 286–299.

Glitza Oliva, I., Tawbi, H., and Davies, M.A. (2017). Melanoma brain metastases: current areas of investigation and future directions. Cancer J. *23*, 68–74.

Greger, J.G., Eastman, S.D., Zhang, V., Bleam, M.R., Hughes, A.M., Smitheman, K.N., Dickerson, S.H., Laquerre, S.G., Liu, L., and Gilmer, T.M. (2012). Combinations of BRAF, MEK, and PI3K/mTOR inhibitors overcome acquired resistance to the BRAF inhibitor GSK2118436 dabrafenib, mediated by NRAS or MEK mutations. Mol. Cancer Ther. *11*, 909–920.

Hidalgo, M., Amant, F., Biankin, A.V., Budinská, E., Byrne, A.T., Caldas, C., Clarke, R.B., de Jong, S., Jonkers, J., Mælandsmo, G.M., et al. (2014). Patient-derived xenograft models: an emerging platform for translational cancer research. Cancer Discov. *4*, 998–1013.

Hodis, E., Watson, I.R., Kryukov, G.V., Arold, S.T., Imielinski, M., Theurillat, J.P., Nickerson, E., Auclair, D., Li, L., Place, C., et al. (2012). A landscape of driver mutations in melanoma. Cell *150*, 251–263.

Holzer, P., Masuya, K., Furet, P., Kallen, J., Valat-Stachyra, T., Ferretti, S., Berghausen, J., Bouisset-Leonard, M., Buschmann, N., Pissot-Soldermann, C., et al. (2015). Discovery of a dihydroisoquinolinone derivative (NVP-CGM097): a highly potent and selective MDM2 inhibitor undergoing phase 1 clinical trials in p53wt tumors. J. Med. Chem. *58*, 6348–6358.

Jeay, S., Gaulis, S., Ferretti, S., Bitter, H., Ito, M., Valat, T., Murakami, M., Ruetz, S., Guthy, D.A., Rynn, C., et al. (2015). A distinct p53 target gene set predicts for response to the selective p53-HDM2 inhibitor NVP-CGM097. eLife *4*, 4.

Kemper, K., Krijgsman, O., Kong, X., Cornelissen-Steijger, P., Shahrabi, A., Weeber, F., van der Velden, D.L., Bleijerveld, O.B., Kuilman, T., Kluin, R.J.C., et al. (2016). BRAF(V600E) kinase domain duplication identified in therapy-refractory melanoma patient-derived Xenografts. Cell Rep. *16*, 263–277.

Krauthammer, M., Kong, Y., Bacchiocchi, A., Evans, P., Pornputtapong, N., Wu, C., McCusker, J.P., Ma, S., Cheng, E., Straub, R., et al. (2015). Exome sequencing identifies recurrent mutations in NF1 and RASopathy genes in sun-exposed melanomas. Nat. Genet. *47*, 996–1002.

Krepler, C., Xiao, M., Sproesser, K., Brafford, P.A., Shannan, B., Beqiri, M., Liu, Q., Xu, W., Garman, B., Nathanson, K.L., et al. (2016). Personalized preclinical trials in BRAF inhibitor-resistant patient-derived xenograft models identify second-line combination therapies. Clin. Cancer Res. *22*, 1592–1602.

Li, L., Fukunaga-Kalabis, M., and Herlyn, M. (2015). Establishing human skin grafts in mice as model for melanoma progression. Methods Mol. Biol. Published online December 13, 2015. https://doi.org/10.1007/7651_2015_301.

Lopez, G.Y., Reitman, Z.J., Solomon, D., Waldman, T., Bigner, D.D., McLendon, R.E., Rosenberg, S.A., Samuels, Y., and Yan, H. (2010). IDH1(R132) mutation identified in one human melanoma metastasis, but not correlated with metastases to the brain. Biochem. Biophys. Res. Commun. *398*, 585–587.

Menzies, A.M., Wilmott, J.S., Drummond, M., Lo, S., Lyle, M., Chan, M.M., Thompson, J.F., Guminski, A., Carlino, M.S., Scolyer, R.A., et al. (2015). Clinicopathologic features associated with efficacy and long-term survival in metastatic melanoma patients treated with BRAF or combined BRAF and MEK inhibitors. Cancer *121*, 3826–3835.

Mondesir, J., Willekens, C., Touat, M., and de Botton, S. (2016). IDH1 and IDH2 mutations as novel therapeutic targets: current perspectives. J. Blood Med. *7*, 171–180.

Monzani, E., Facchetti, F., Galmozzi, E., Corsini, E., Benetti, A., Cavazzin, C., Gritti, A., Piccinini, A., Porro, D., Santinami, M., et al. (2007). Melanoma contains CD133 and ABCG2 positive cells with enhanced tumourigenic potential. Eur. J. Cancer *43*, 935–946.

Nazarian, R., Shi, H., Wang, Q., Kong, X., Koya, R.C., Lee, H., Chen, Z., Lee, M.-K.K., Attar, N., Sazegar, H., et al. (2010). Melanomas acquire resistance to B-RAF(V600E) inhibition by RTK or N-RAS upregulation. Nature *468*, 973–977.

Némati, F., Sastre-Garau, X., Laurent, C., Couturier, J., Mariani, P., Desjardins, L., Piperno-Neumann, S., Lantz, O., Asselain, B., Plancher, C., et al. (2010). Establishment and characterization of a panel of human uveal melanoma xenografts derived from primary and/or metastatic tumors. Clin. Cancer Res. *16*, 2352–2362.

Peng, W., Chen, J.Q., Liu, C., Malu, S., Creasy, C., Tetzlaff, M.T., Xu, C., McKenzie, J.A., Zhang, C., Liang, X., et al. (2016). Loss of PTEN promotes resistance to T cell-mediated immunotherapy. Cancer Discov. *6*, 202–216.

Quintana, E., Shackleton, M., Sabel, M.S., Fullen, D.R., Johnson, T.M., and Morrison, S.J. (2008). Efficient tumour formation by single human melanoma cells. Nature *456*, 593–598.

Quintana, E., Piskounova, E., Shackleton, M., Weinberg, D., Eskiocak, U., Fullen, D.R., Johnson, T.M., and Morrison, S.J. (2012). Human melanoma metastasis in NSG mice correlates with clinical outcome in patients. Sci. Transl. Med. *4*, 159ra149.

Rizos, H., Menzies, A.M., Pupo, G.M., Carlino, M.S., Fung, C., Hyman, J., Haydu, L.E., Mijatov, B., Becker, T.M., Boyd, S.C., et al. (2014). BRAF inhibitor resistance mechanisms in metastatic melanoma: spectrum and clinical impact. Clin. Cancer Res. *20*, 1965–1977.

Rongvaux, A., Willinger, T., Martinek, J., Strowig, T., Gearty, S.V., Teichmann, L.L., Saito, Y., Marches, F., Halene, S., Palucka, A.K., et al. (2014). Development and function of human innate immune cells in a humanized mouse model. Nat. Biotechnol. *32*, 364–372.

Rygaard, J., and Povlsen, C.O. (1969). Heterotransplantation of a human malignant tumour to "Nude" mice. Acta Pathol. Microbiol. Scand. *77*, 758–760.

Sanmamed, M.F., Chester, C., Melero, I., and Kohrt, H. (2016). Defining the optimal murine models to investigate immune checkpoint blockers and their combination with other immunotherapies. Ann. Oncol. *27*, 1190–1198.

Schadendorf, D., Hodi, F.S., Robert, C., Weber, J.S., Margolin, K., Hamid, O., Patt, D., Chen, T.-T.T., Berman, D.M., and Wolchok, J.D. (2015). Pooled analysis of long-term survival data from phase II and phase III trials of ipilimumab in unresectable or metastatic melanoma. J. Clin. Oncol. *33*, 1889–1894.

Segura, M.F., Fontanals-Cirera, B., Gaziel-Sovran, A., Guijarro, M.V., Hanniford, D., Zhang, G., González-Gomez, P., Morante, M., Jubierre, L., Zhang, W., et al. (2013). BRD4 sustains melanoma proliferation and represents a new target for epigenetic therapy. Cancer Res. *73*, 6264–6276.

Shannan, B., Chen, Q., Watters, A., Perego, M., Krepler, C., Thombre, R., Li, L., Rajan, G., Peterson, S., Gimotty, P.A., et al. (2016). Enhancing the evaluation of PI3K inhibitors through 3D melanoma models. Pigment Cell Melanoma Res. *29*, 317–328.

Sheng, X., Kong, Y., Li, Y., Zhang, Q., Si, L., Cui, C., Chi, Z., Tang, B., Mao, L., Lian, B., et al. (2016). GNAQ and GNA11 mutations occur in 9.5% of mucosal melanoma and are associated with poor prognosis. Eur. J. Cancer *65*, 156–163.

Shi, H., Hugo, W., Kong, X., Hong, A., Koya, R.C., Moriceau, G., Chodon, T., Guo, R., Johnson, D.B., Dahlman, K.B., et al. (2014). Acquired resistance and clonal evolution in melanoma during BRAF inhibitor therapy. Cancer Discov. *4*, 80–93.

Staudt, M., Lasithiotakis, K., Leiter, U., Meier, F., Eigentler, T., Bamberg, M., Tatagiba, M., Brossart, P., and Garbe, C. (2010). Determinants of survival in patients with brain metastases from cutaneous melanoma. Br. J. Cancer *102*, 1213–1218.

Tateishi, K., Wakimoto, H., Iafrate, A.J., Tanaka, S., Loebel, F., Lelic, N., Wiederschain, D., Bedel, O., Deng, G., Zhang, B., et al. (2015). Extreme vulnerability of IDH1 mutant cancers to NAD+ depletion. Cancer Cell *28*, 773–784.

Tibes, R., Qiu, Y., Lu, Y., Hennessy, B., Andreeff, M., Mills, G.B., and Kornblau, S.M. (2006). Reverse phase protein array: validation of a novel proteomic technology and utility for analysis of primary leukemia specimens and hematopoietic stem cells. Mol. Cancer Ther. *5*, 2512–2521.

Townsend, E.C., Murakami, M.A., Christodoulou, A., Christie, A.L., Köster, J., DeSouza, T.A., Morgan, E.A., Kallgren, S.P., Liu, H., Wu, S.C., et al. (2016). The public repository of xenografts enables discovery and randomized phase II-like trials in mice. Cancer Cell *29*, 574–586.

Van Raamsdonk, C.D., Griewank, K.G., Crosby, M.B., Garrido, M.C., Vemula, S., Wiesner, T., Obenauf, A.C., Wackernagel, W., Green, G., Bouvier, N., et al. (2010). Mutations in GNA11 in uveal melanoma. N. Engl. J. Med. *363*, 2191–2199.

Villanueva, J., Vultur, A., Lee, J.T., Somasundaram, R., Fukunaga-Kalabis, M., Cipolla, A.K., Wubbenhorst, B., Xu, X., Gimotty, P.A., Kee, D., et al. (2010). Acquired resistance to BRAF inhibitors mediated by a RAF kinase switch in melanoma can be overcome by cotargeting MEK and IGF-1R/PI3K. Cancer Cell *18*, 683–695.

Villanueva, J., Infante, J.R., Krepler, C., Reyes-Uribe, P., Samanta, M., Chen, H.Y., Li, B., Swoboda, R.K., Wilson, M., Vultur, A., et al. (2013). Concurrent MEK2 mutation and BRAF amplification confer resistance to BRAF and MEK inhibitors in melanoma. Cell Rep. *4*, 1090–1099.